


Helical Shear-Flow Stabilization of an Astrophysically Relevant Laboratory Plasma JetEric Sander Lavine^{*} and Setthivoine You[†]*University of Washington, William E. Boeing department of Aeronautics and Astronautics, Seattle, Washington 98105, USA* (Received 7 August 2018; revised manuscript received 3 April 2019; published 4 October 2019)

Astrophysical jets are collimated, high-speed outflows observed to be natural features of celestial objects that spin and accrete matter. From protoplanetary nebula and young stellar objects to active galactic nuclei, common features suggest that universal mechanisms may lead to the remarkable straightness observed in many jets. Here we report observations from a new astrophysically relevant laboratory plasma jet experiment demonstrating the formation of long-lived, collimated, high aspect-ratio jets. The magnetized jets have strong helical shear flows and remain stable to instabilities over many growth times. These observations corroborate theoretical predictions that strong helical shear flows can stabilize current-driven instabilities in magnetically confined plasmas, solar prominences, and magnetically driven astrophysical jets in nature.

DOI: [10.1103/PhysRevLett.123.145002](https://doi.org/10.1103/PhysRevLett.123.145002)

Several models have been proposed to explain the remarkable degree of collimation observed in astrophysical jets. Theoretical [1] and laboratory [2] hydrodynamic models suppose that polar funnels in a thick accretion disk behave as nozzles with high Mach number radiative flows responsible for collimation beyond the formation region [3]. These models, however, have difficulty explaining the collimation of very long jets observed from low aspect-ratio funnels [4], overdense jets surrounded by vacuum or low density medium [5], observed signatures of helical motion [6], or helical magnetic fields [7]. Therefore, theoretical [8] and laboratory [9] magnetohydrodynamic (MHD) models include magnetic fields for jet launching and collimation. These magnetized jets are generally treated as azimuthally symmetric z pinches or screw pinches, both of which are susceptible to current-driven instabilities [10]. Laboratory experiments designed to produce such jets have therefore generally resulted in short-lived, collimated jets [11] with instabilities twisting and breaking the column at critical aspect ratios [12].

Sufficiently sheared axial flows were predicted to improve the stability of z pinches [13], and experiments have verified these predictions in jets dominated by axial current [14–16]. The mechanism responsible for stabilization is a mode mixing where each perturbed nested flux surface is convected by flow perpendicular to the radial growth direction. A flow shear between flux surfaces of the order of the growth rate of the perturbation (Alfvén velocity v_a times the axial mode number k_z of the perturbation) is sufficient to destroy the coherence of the mode. Assuming a pressure profile such that pressure-driven instabilities can be neglected, sheared flow in the azimuthal direction is also predicted to provide stability (to nonaxisymmetric perturbations) in z -pinch plasmas by imposing a radial

dependence on the phase of the azimuthal angle [17]. By combining azimuthal and axial sheared flows to produce helically sheared flows, linear stability analysis of z -pinch plasmas predicts a more effective reduction in nonaxisymmetric current-driven instabilities than with sheared axial flow alone [17].

In screw-pinch plasmas where the magnetic field is helical and not azimuthal as in a z pinch, radial perturbations are convected in a helical manner. There are therefore just two ways to render the perturbations incoherent: helical magnetic shear and helical flow shear. Axial flow shear by itself is not enough, as that would only mode mix in one direction, leaving the other direction to be coherent and grow. Here we report observations from a new astrophysically relevant laboratory plasma jet experiment [18] demonstrating the formation of long-lived, collimated, high aspect-ratio jets. The experiment uses nested, planar, magnetized plasma guns with azimuthally symmetric gas slits to produce dense jets far from the walls, with embedded axial magnetic fields and strong helical shear flows. The jets are stable to current-driven instabilities over many growth times despite occupying classically unstable space. These results corroborate the hypothesis that strong helical shear flows enhance the stability of magnetically driven jets with helical fields, providing one possible mechanism for the incredible aspect ratios observed in naturally occurring magnetized plasma jets.

If magnetically driven jets obey MHD scaling laws [19], then times should scale as $a\sqrt{b/c}$, velocities as $\sqrt{c/b}$, and magnetic fields as \sqrt{c} , where a is the ratio of jet radii, b is the ratio of mass densities, and c is the ratio of the plasma pressures. For our laboratory experiment [18], these parameters agree with those of typical protostellar jets [11] to within an order of magnitude (Table I). However,

TABLE I. Comparison of experimental and astrophysical jet parameters.

Parameter	LabJet ^a	YSO jet ^b
Radius (cm)	2–10	10^{15}
Length (cm)	110	10^{17}
Density (g m^{-3})	10^{-6} –0.1	10^{-14} – 10^{-12}
Temperature (eV)	1–20 ^c	0.5–100
Pressure (Torr)	0.006–600	10^{-11}
Magnetic field (T)	0.01–0.5	3×10^{-7} –0.3
Timescale (s)	10^{-6} – 10^{-4}	10^{11} – 10^{13}
Axial velocity (km/s)	30–80	100–500
Azimuthal velocity (km/s)	0–80	10–30
Mean-free path (cm)	0.01	10^9
Re_m	$\sim 10^3$	$> 10^{15}$
Re	$\sim 10^4$	$> 10^8$
Pe	$\sim 10^3$	$> 10^7$

^aReference [18].

^bReference [11].

^cFrom Doppler broadening.

because jets in nature vary widely in physical parameters as well as dimensionless numbers such as Reynolds (Re), magnetic Reynolds (Re_m), and Peclet (Pe) numbers [9,11,19,20], it is likely that boundary conditions play a significant role in addition to dimensionless numbers in jet dynamics and evolution. Our experimental setup therefore uses the simplest feasible design to mimic the boundary conditions of a magnetic tower astrophysical jet [8]. In such a model, a poloidal magnetic field from a magnetized

central object is frozen into a differentially rotating accretion disk. Continued winding increases the azimuthal field and magnetic pressure, driving expansion of a jet along the rotation axis. To simulate these conditions in a laboratory, the experiment [Fig. 1(a)] uses three concentric, planar, and annular electrodes threaded by a vacuum dipole magnetic field. Independent biasing of the inner two electrodes with respect to the outer electrode provides control of the radial electric field profile. This design approximates an accretion disk rotating azimuthally in a poloidal magnetic field and provides a control knob on the azimuthal rotation profile, $u_\phi \sim -E_r(r)/B_z(r)$. The two concentric cathodes also drive different poloidal currents, $\mathbf{j}_{\text{pol}}(r)$, which provides some degree of control on the axial flow shear $u_z(r)$ [21]. We also pay careful attention to providing an azimuthally symmetric mass source by injecting the working gas (hydrogen typically) through four annular slits in the electrodes. Symmetry at the foot point of the jet is necessary for the plasma to rotate freely, unhindered by a discrete number of gas holes. The vacuum chamber is not prefilled with gas and has a base pressure of $\sim 10^{-7}$ Torr. The opposite end of the vacuum chamber holds an unused planar plasma gun that is electrically isolated from the grounded vacuum chamber. Our triple electrode design with azimuthally symmetric gas slits improves on a previous apparatus that has a double electrode setup and discrete gas holes [22].

The evolution of the laboratory plasma jet can be divided into three distinct stages: stage I with a small jet, stage II with a diffuse plume, and stage III with a big jet [Fig. 1(d)].

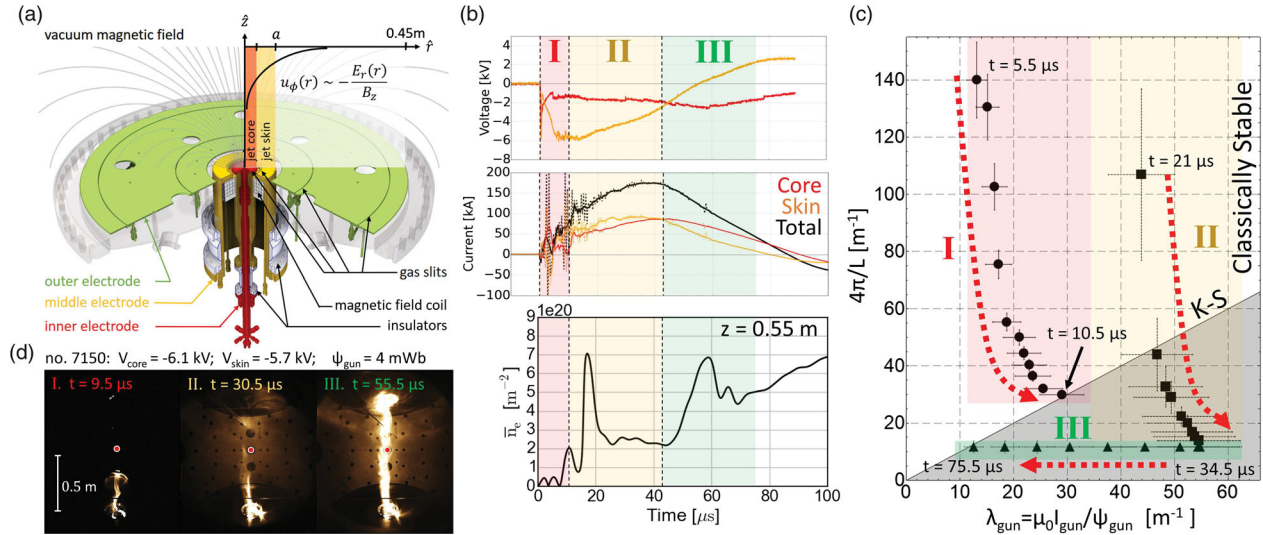


FIG. 1. (a) Novel triple electrode plasma gun designed to replicate the basic configuration of an accretion disk around a magnetized central engine. (b) Voltage, current, and electron density measured using high-voltage probes, Rogowski coils, and a heterodyne interferometer [path delineated by red dots at $z = 54$ cm in (d)]. Shaded regions indicate the duration of the three distinct formation stages. (c) Jet evolution through classical stability space. The initial jet goes unstable upon reaching the Kruskal-Shafranov (K-S) kink condition (gray shaded region). The second jet forms in stable space but crosses into classically unstable space as it lengthens and the current ramps up. The long, collimated jet remains stable for $\sim 35 \mu\text{s}$ as the current decreases. (d) High-speed camera images of the three distinct evolutionary stages of the laboratory plasma jet.

Stage I begins when the gas breaks down along magnetic field lines connecting the inner and middle gas slits to the outer slits. These azimuthally continuous nested arches (nested Bundt cakes) have parallel flowing currents which cause them to zipper up into a jet along the central axis [Fig. 1(d), frame 1]. The stage I jet lengthens into the vacuum chamber, then rapidly develops a helical kink instability at the ideal Kruskal-Shafranov threshold [23] [Fig. 1(c) and Fig. 1(d), frame 1)] This instability criterion can be expressed as [12] $\lambda_{\text{gun}} > 4\pi/L$, where $\lambda_{\text{gun}} = \mu_0 I_{\text{gun}}/\psi_{\text{gun}}$ is the total gun current I_{gun} normalized to the vacuum magnetic flux $\psi_{\text{gun}} \sim 4 \text{ mWb}$ and L is the jet length. The vacuum permeability is μ_0 . We use a high-speed camera to infer the approximate radial and axial extent of the plasma jet, assuming optical emission is proportional to the square of the plasma density. An interferometer measures densities of $\sim 10^{22} \text{ m}^{-3}$ in the plasma jet [24] [Fig. 1(b)]. Steep density gradients between the dense plasma and vacuum background result in sharp boundaries in the plasma emission. The gun currents and vacuum magnetic field coil currents are measured with Rogowski coils and commercial pulsed current monitors to give the evolution of the jet in classical stability space [Fig. 1(c)]. The current is also inferred from an *in situ*, linear \dot{B} probe array [18,25]. Measurements at various axial positions show that all of the gun current (to experimental certainty) remains in the plasma jet over the full discharge duration; however, as the jet evolves into stages II and III, the magnetic field configuration may become more complex than the initially assumed screw pinch. This is the focus of another paper. Following the kink instability, the stage I jet undergoes magnetic reconnection [26], detaches from the plasma gun, and propagates away from the electrodes into the vacuum chamber (see videos in Supplemental Material [27]). The stage I jet evolves over a few Alfvén times ($< 10 \mu\text{s}$ total) and confirms earlier laboratory jet experiments [12,28].

Stage II is a transition period lasting 3 times longer than stage I. Unlike stage I, which formed into a vacuum, the new formation begins as a diffuse plume which expands into the remains of the ejected stage I plasma [Fig. 1(d), frame 2]. The plume density is approximately half of the stage I jet [Fig. 1(b)] and increases with the current as the plume collimates and lengthens. The trajectory in stability space shows that the plume begins in the classically stable region but crosses into the classically unstable region [Fig. 1(c)]. As opposed to the stage I jets that propagate at Alfvénic velocities (probably with axial shear flows driven by nonuniform $\mathbf{j} \times \mathbf{B}$ forces), the stage II jet develops less rapidly than the Alfvénic timescales, presumably allowing for the azimuthal component of the flow to develop on $\mathbf{E} \times \mathbf{B}$ timescales as it expands.

Stage III begins when the gun current driving the core of the jet becomes larger than the gun current driving the skin. In shot no. 7150, this occurs at $t \approx 40 \mu\text{s}$ [Fig. 1(b)]. At this

point, the jet has an aspect ratio of $\sim 20:1$ with a length of $\sim 1.1 \text{ m}$ (limited by the length of the vacuum chamber), an apparent radius of $\sim 5 \text{ cm}$, and carries 50–160 kA of current. This jet remains stable for $\sim 35 \mu\text{s}$, more than 3 times longer than the stage I jet, despite occupying classically unstable space [Fig. 1(c)]. The density in the stage III jets rises to similar or greater levels than the dense stage I jets, suggesting strong continual pumping of particles from the foot points [21,28,29]. With measured densities of $\sim 10^{22} \text{ m}^{-3}$ and magnetic field strengths of $\sim 0.4 \text{ T}$, the shortest growth time for the kink instability (corresponding to $k_z r_0 = \pi$, where r_0 is the jet radius) is $\sim 0.2 \mu\text{s}$, so the stage III jet is stable for $\gtrsim 180$ growth times and appears to be limited only by the power available in the gun driving systems.

High-speed videos of the long, stable jets suggest strong axial and azimuthal flows (see videos in Supplemental Material [27]). A custom optical fiber bundle with 94 chords arranged in two perpendicular planes around the center of the spherical vacuum chamber collects ion spectral lines [Figs. 2(a) and 2(b)]. The C II 723.64 nm impurity spectra are recorded with a $1 \mu\text{s}$ exposure time using a PI-MAX3 intensified CCD camera mounted to a 1 m focal length monochromator with a 2400 l/mm grating. Because the ion-impurity equipartition time is small (on the order of the ion-ion collision time $\sim 2 \text{ ns}$) compared to the dynamical timescales, the bulk plasma and impurities are assumed to have similar properties [30,31]. The spectroscopic Doppler measurements (Fig. 2 in Supplemental Material [27]) reveal line-integrated axial flows up to 50 km/s and azimuthal flows up to 20 km/s in the counterclockwise ($+\phi$) direction. The azimuthal flow is consistent with the $\mathbf{E} \times \mathbf{B}$ direction, where the electric field points radially inward and the vacuum magnetic field points out of the gun. A simple helical shear-flow model (Fig. 3 of Supplemental Material [27]) fitted to spectroscopic Doppler data provides one estimate of the local flow profile. The model consists of two nested cylindrical regions of equal thickness and independent azimuthal velocity v_ϕ . The jet center position and diameter in the central midplane are determined by Gaussian fits to the binned intensity, with adjustments for uncertainties in the jet center and radius. Because flow features appear to be convected together in the axial direction, the axial flow velocity profile is assumed to be a flattop exponential that goes to zero at the jet radius. Two final parameters represent any bulk motion of the plasma jet due to gyration. Assuming uniform emissivity inside the plasma and zero emissivity outside, line-integrated velocities through the plasma model are compared to the observed line-integrated velocities in both measurement planes [Fig. 2(d)]. The results suggest that the flows in the stage III jet are helically sheared and well represented to first order by the simple double shell model. For shot no. 7150 at $t = 59 \mu\text{s}$, the average core azimuthal velocity in the model is $\sim 28 \text{ km/s}$, the skin azimuthal velocity is $\sim 10 \text{ km/s}$, and the axial

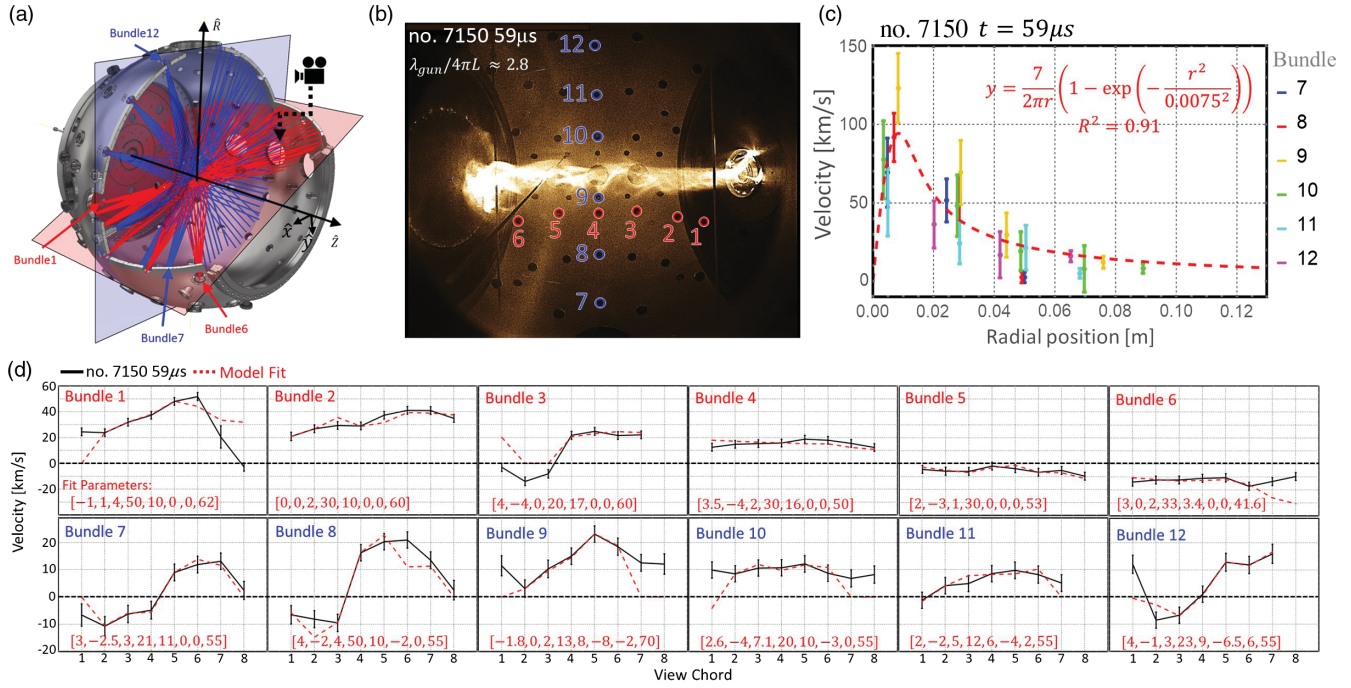


FIG. 2. Multichannel optical spectroscopy on the MOCHI experiment. (a) 94 view chords arranged into two planes, bundles 1–6 in the poloidal measurement plane (red), and bundles 7–12 in the toroidal plane (blue). (b) Fast imaging frame of the stable, collimated plasma jet from shot no. 7150 at 59 μs . (c) Lamb-Oseen vortex fit to the collective Abel inverted azimuthal velocity profiles. The best fit predicts the center of the jet in the toroidal plane is located at $(x, y) = (-2, -0.2)$ cm. (d) Double shell spectroscopy model fits to the observed CII line-integrated Doppler shifts. Model fit parameters in red are listed as follows: $[\Delta x, \Delta y, \Delta r_0, v_{\phi\text{core}}, v_{\phi\text{skin}}, v_x, v_y, v_{0\text{axial}}]$ with lengths in units of cm and velocities in units of km/s. The model start location and radius is $(x, y, r_0) = (-4.7, -2.4, 3.5)$ as determined by Gaussian fits to the binned intensity.

velocity is ~ 56 km/s. The jet is well collimated, straight, and stable [Fig. 2(b)] despite being in classically unstable parameter space with $\lambda_{\text{gun}}/4\pi L \approx 2.8$. The axial flow shear in the model can be compared to the threshold for wall-free stabilization, $v'_z > 0.1 k_z v_a$ [13], where $v'_z = dv_z/dr$. For an average radius of 6.4 cm, the axial flow shear between $3.06 < r < 6.14$ cm is sufficient to stabilize the fastest growing kink mode, with a peak value ~ 8 times larger than the threshold.

Abel inversion with the plasma partitioned into radial zones with constant emissivity and azimuthal velocity (Fig. 4 of Supplemental Material [27]) provides another estimate of the azimuthal velocity profile [32]. Each viewing chord in the azimuthal measurement plane is assumed to be orthogonal to the jet axis such that the line-integrated velocity along each line of sight is due only to azimuthal rotation. Two free parameters control the jet center location and are adjusted to maximize the R^2 value of a Lamb-Oseen vortex flow best fit line. A vortex profile was selected because it was the only flow profile to fully stabilize the kink mode in a linear stability analysis [17] and because the double shell model suggests a centrally peaked velocity profile. For shot 7150, we obtain the best fit for a jet center location $(x, y) = (-2, -0.2)$ cm from the chamber center. The peak azimuthal velocity of the fit is approximately equivalent to the experimental Alfvén velocity.

Experimentally inferred rotation profiles are compared to the theoretical profiles of Ref. [17] (rigid rotor, quadratic, and vortex) in Fig. 3. We observe that the shear for both our models generally bounds that of the ideal vortex flow and far exceeds that of the quadratic flow profile which was unstable [Fig. 3(b)]. For an Alfvén velocity of ~ 83 km/s and a jet radius of 6.4 cm, the ideal vortex flow profile is theoretically stable to kink instabilities with an axial wavelength ≥ 6.7 cm, which is less than the minimum

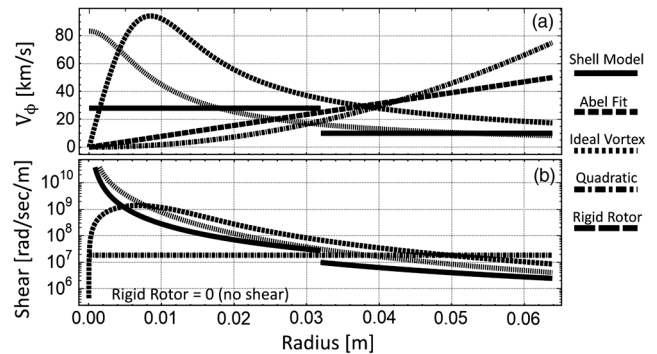


FIG. 3. (a) Comparison of experimentally inferred flow profiles to various azimuthal flows considered in Ref. [17]. (b) Shear profiles of the corresponding azimuthal flows.

possible value of 12.8 cm ($2r_0$). The addition of sheared axial flow is predicted to further improve stability.

A kinklike instability appears to develop only towards the end of the discharge as the gun current decreases from 160 to 50 kA. This is contrary to the expectation that a classical current-carrying magnetized jet with no flows should become more stable with decreasing axial current. Because currents are ultimately responsible for the $\mathbf{j} \times \mathbf{B}$ forces that drive stabilizing helical flows, in competition with driving destabilizing magnetic $\mathbf{j} \times \mathbf{B}$ forces, we speculate that as the current decreases during the stage III jet, the stabilizing effect of helical shear flows weakens more rapidly than the destabilizing effect of helical magnetic fields. This would explain why the kinklike instabilities only appear near the end of the discharge. The influence of nonideal effects, including both resistive and line tying effects at the electrodes [33], warrants further investigation.

In summary, our observations demonstrate how helical flow shear in magnetically driven jets is one possible mechanism for attaining large aspect ratios while remaining stable to free-boundary MHD instabilities. The long, collimated jets in this experiment remain stable for $\gtrsim 140$ –180 instability growth times despite occupying classically unstable space and appear to be limited only by the power available in the gun driving systems. Compared to earlier laboratory plasma jet experiments, our nested plasma gun configuration more accurately reproduces the essential boundary conditions of an accretion disk around a magnetized central engine. This unique triple electrode setup with azimuthally symmetric gas slits appears necessary and sufficient to drive strong, azimuthal and axial flow shear, supporting the conjecture that sufficient helical flow shear can stabilize magnetized plasma jets in a vacuum.

This work was supported by the U.S. DOE Grant No. DE-SC0010340.

*Present address: Cornell University, Laboratory of Plasma Studies, Cornell Engineering, Ithaca, New York 14853 USA.

esl97@cornell.edu

†Present address: Graduate School of Frontier Sciences, University of Tokyo, Tokyo 113-0032, Japan.

you@ts.t.u-tokyo.ac.jp

- [1] V. Icke, G. Mellema, B. Balick, F. Eulerink, and A. Frank, *Nature (London)* **355**, 524 (1992).
- [2] B. A. Remington, R. P. Drake, and D. D. Ryutov, *Rev. Mod. Phys.* **78**, 755 (2006).
- [3] M. L. Norman, K.-H. A. Winkler, L. Smarr, and M. D. Smith, *Astron. Astrophys.* **113**, 285 (1982).
- [4] D. S. De Young, *Science* **252**, 389 (1991).
- [5] A. Frank, D. Ryu, T. W. Jones, and A. Noriega-Crespo, *Astrophys. J. Lett.* **494**, L79 (1998).
- [6] A. E. Broderick and A. Loeb, *Astrophys. J. Lett.* **703**, L104 (2009).
- [7] K. Asada, M. Inoue, Y. Uchida, S. Kameno, K. Fujisawa, S. Iguchi, and M. Mutoh, *Publ. Astron. Soc. Jpn.* **54**, L39 (2002).
- [8] D. Lynden-Bell, *Mon. Not. R. Astron. Soc.* **341**, 1360 (2003).
- [9] P. M. Bellan, S. You, and S. C. Hsu, *Astrophys. Space Sci.* **298**, 203 (2005).
- [10] J. P. Freidberg, *Ideal MHD* (Cambridge University Press, Cambridge, England, 2014).
- [11] A. Ciardi, in *Lecture Notes in Physics*, edited by P. J. V. Garcia and J. M. Ferreira (Springer-Verlag, Berlin, 2010), Vol. 793, p. 31.
- [12] S. C. Hsu and P. M. Bellan, *Phys. Plasmas* **12**, 032103 (2005).
- [13] U. Shumlak and C. W. Hartman, *Phys. Rev. Lett.* **75**, 3285 (1995).
- [14] U. Shumlak, R. P. Golingo, B. A. Nelson, and D. J. Den Hartog, *Phys. Rev. Lett.* **87**, 205005 (2001).
- [15] Y. Zhang, M. Gilmore, S. C. Hsu, D. M. Fisher, and A. G. Lynn, *Phys. Plasmas* **24**, 110702 (2017).
- [16] Y. Zhang, D. M. Fisher, M. Gilmore, S. C. Hsu, and A. G. Lynn, *Phys. Plasmas* **25**, 055709 (2018).
- [17] L. F. Wanex, V. I. Sotnikov, and J. N. Leboeuf, *Phys. Plasmas* **12**, 042101 (2005).
- [18] S. You, J. von der Linden, E. S. Lavine, E. G. Carroll, A. Card, M. Quinley, and M. Azuara-Rosales, *Astrophys. J. Suppl. Ser.* **236**, 29 (2018).
- [19] D. D. Ryutov, R. P. Drake, and B. A. Remington, *Astrophys. J. Suppl. Ser.* **127**, 465 (2000).
- [20] S. V. Lebedev, J. P. Chittenden, F. N. Beg, S. N. Bland, A. Ciardi, D. Ampleford, S. Hughes, M. G. Haines, A. Frank, E. G. Blackman, and T. Gardiner, *Astrophys. J.* **564**, 113 (2002).
- [21] P. M. Bellan, *Phys. Plasmas* **10**, 1999 (2003).
- [22] S. C. Hsu and P. M. Bellan, *Mon. Not. R. Astron. Soc.* **334**, 257 (2002).
- [23] M. Kruskal and J. L. Tuck, *Proc. R. Soc. A* **245**, 222 (1958).
- [24] A. H. Card, Implementation of an unequal path length, heterodyne interferometer on the MOCHI LabJet experiment, Master's thesis, University of Washington, 2017.
- [25] E. S. Lavine, The evolution and dynamics of magnetized plasma jets in the MOCHI LabJet experiment, Ph. D. thesis, University of Washington, 2018.
- [26] A. L. Moser and P. M. Bellan, *Nature (London)* **482**, 379 (2012).
- [27] See Supplemental Material at <http://link.aps.org/supplemental/10.1103/PhysRevLett.123.145002> for high-speed videos, high-speed camera images of large aspect-ratio jets, sample Ion Doppler spectroscopy lineouts, geometry of double-shell spectroscopy model, geometry of Abel inversion technique.
- [28] G. S. Yun, S. You, and P. M. Bellan, *Nucl. Fusion* **47**, 181 (2007).
- [29] S. You, G. S. Yun, and P. M. Bellan, *Phys. Rev. Lett.* **95**, 045002 (2005).
- [30] I. H. Hutchinson, *Principles of Plasma Diagnostics*, 2nd ed. (Cambridge University Press, Cambridge, England, 2002).
- [31] M. G. von Hellermann and H. P. Summers, *Rev. Sci. Instrum.* **63**, 5132 (1992).
- [32] R. E. Bell, *Rev. Sci. Instrum.* **68**, 930 (1997).
- [33] I. Furno, T. P. Intrator, G. Lapenta, L. Dorf, S. Abbate, and D. D. Ryutov, *Phys. Plasmas* **14**, 022103 (2007).